Numerical study on the electron–wall interaction in a Hall thruster with segmented electrodes placed at the channel exit*

Qing Shao-Wei(卿绍伟)[a)†], E Peng(鄂 鹏)[b)], Duan Ping(段 萍)[c)], and Xu Dian-Guo(徐殿国)[b)]

[a)] *Power Engineering Institute, Chongqing University, Chongqing* 400044, *China*
[b)] *Department of Electrical Engineering, Harbin Institute of Technology, Harbin* 150001, *China*
[c)] *School of Physics, Dalian Maritime University, Dalian* 116026, *China*

(Received 23 October 2012; revised manuscript received 7 January 2013)

Electron–wall interaction is always recognized as an important physical problem because of its remarkable influences on thruster discharge and performance. Based on existing theories, an electrode is predicted to weaken electron–wall interaction due to its low secondary electron emission characteristic. In this paper, the electron–wall interaction in an Aton-type Hall thruster with low-emissive electrodes placed near the exit of discharge channel is studied by a fully kinetic particle-in-cell method. The results show that the electron–wall interaction in the region of segmented electrode is indeed weakened, but it is significantly enhanced in the remaining region of discharge channel. It is mainly caused by electrode conductive property which makes equipotential lines convex toward channel exit and even parallel to wall surface in near-wall region; this convex equipotential configuration results in significant physical effects such as repelling electrons, which causes the electrons to move toward the channel center, and the electrons emitted from electrodes to be remarkably accelerated, thereby increasing electron temperature in the discharge channel, etc. Furthermore, the results also indicate that the discharge current in the segmented electrode case is larger than in the non-segmented electrode case, which is qualitatively in accordance with previous experimental results.

Keywords: Hall thruster, electron–wall interaction, segmented electrodes, particle simulation

PACS: 52.65.Rr, 52.75.–d **DOI:** 10.1088/1674-1056/22/8/085203

1. Introduction

The Hall thruster is one of the most advanced space electric propulsion devices, which generates the thrust by axial electrostatic acceleration of ions in quasineutral plasma.[1,2] The ion is produced due to the ionizing collision between atom and electron with relative high temperature. As a whole, the electron temperature depends on the joule heating of axial electric field and the energy loss in the processes of electron–wall and electron–atom interactions. It thus suggests that the electron–wall interaction is an important factor influencing the ionization rate of propellant atom in Hall thruster. The electron–wall interaction also has other influence on the discharge performance of Hall thruster. The most well-known one is the so-called electron near wall conductivity (NWC) which has been developed since the 1960s.[3,4] The electron NWC occurs because electron–wall interaction destroys the steady Hall drift of electron in $\boldsymbol{E}\times\boldsymbol{B}$ direction (where $\boldsymbol{E}$ and $\boldsymbol{B}$ are axial electric and radial magnetic fields, respectively), which is believed to be responsible for the portion of electron conductivity that is higher than classical value.[4,5] We then can come to a conclusion that the electron NWC caused by electron–wall interaction increases electron current, and thus reducing the discharge efficiency. Moreover, the electron–wall interaction has other influences on the discharge of Hall thruster, such as the potential distribution in discharge channel,[6] the wall temperature effect caused by the energy deposition of incident electron moving toward lateral walls, etc.[7]

It has been recognized that wall secondary electron emission (SEE) is a notable influence factor of electron–wall interaction by reducing the potential drop of near-wall sheath.[8] The increased incident electron flux $\Gamma_{\rm e}$ at wall is balanced by the ion flux $\Gamma_{\rm i}$ and secondary electron flux $\Gamma_{\rm se}$, and satisfies the relationship $\Gamma_{\rm e}=\Gamma_{\rm i}/(1-\delta)$, where $\delta=\Gamma_{\rm se}/\Gamma_{\rm e}$ called total SEE yield. As δ reaches approximately unit, the sheath enters into space-charge saturated (SCS) regime, and the wall acts as an extremely effective particle and energy sink.[6,8]

Both experimental and numerical studies also have indicated that the SEE of channel walls has significant effects on thruster discharge and performance.[9–12] These investigations attribute the influence of SEE to two ways. (i) It decreases sheath potential drop, thereby increasing the deposition of primary electron energies on walls;[8] meanwhile, the emitted secondary electrons, with much lower energies than primary electrons, are involved into the discharge, reducing the bulk temperature and so the ionization rate. (ii) It gives rise to high cross-field conductivity near the walls, consequently af-

*Project supported by the Fundamental Research Funds for the Central Universities, China (Grant No. 0903005203189), the National Natural Science Foundation of China (Grant Nos. 11005025, 10975026, and 11275034), the Scientific Research Innovation Foundation of Harbin Institution of Technology, China (Grant No. HITNSRIF2009044), and the Key Project of the Scientific Technology Program of Liaoning Province, China (Grant No. 2011224007).

†Corresponding author. E-mail: qshaowei@gmail.com

© 2013 Chinese Physical Society and IOP Publishing Ltd

fecting the electric potential distribution and ion acceleration process.[10]

As the SEE yield of a conductive wall is generally much lower than that of a dielectric wall, especially, the SEE yield of a metal wall can be negligible,[10,12] the segmented electrodes are proposed as a promising way to control the plasma flow and enhance thruster performance.[13–15] It has been demonstrated that segmented electrodes with several millimeters in length placed near the thruster exit can remarkably increase electron temperature, increase discharge current, change electric potential distribution, and narrow plasma plume at low gas flow rate.[12,16] Although the effects of low-emissive segmented electrodes have been well documented, the electron–wall interaction and the relative effects in the discharge channel of Hall thruster are not stressed sufficiently. Moreover, it is also needed to evaluate the segmented electrodes used in other kinds of Hall thrusters, such as Aton[17,18] involved in this paper.

In this paper, we present the detailed numerical results of how the length of low-emissive electrodes near the exit of a 1-kW Aton-type Hall thruster affects the distributions of secondary electron flux, electron temperature, electric potential, ionization rate, and discharge current, by a fully kinetic two-dimensional (2D) particle-in-cell (PIC) model for a low gas flow rate of 2 mg/s. The remaining parts of this paper are organized as follows. In Section 2, the numerical model is depicted in detail. In Section 3, the results of low-emissive electrodes are presented, and the reason for electron–wall interaction enhancement caused by segmented electrodes is discussed. Finally some conclusions are given in Section 4.

2. Numerical model

The numerical model has been described in detail elsewhere.[19] Here we briefly review some main points of the model. The simulated Hall thruster in this paper is a 1-kW Aton type which has an outer diameter of 71 mm, a channel width of 14 mm and a channel length of 30 mm.[17,18] Figure 1 shows the computational region. It involves two-dimensional cylindrical coordinates (r, z), where r and z represent radial and axial directions, respectively. The anode is located on the left boundary. Ions are ejected from the right boundary. As the cathode is located outside the discharge channel, the right boundary is also a virtual cathode. Seed electrons are introduced into the channel from here, with the number per time step Δt determined by a quasi-neutral injection method.[20] The two lateral (inner and outer) walls are made up of both boron nitride (BN) ceramic and segmented electrodes, with the electrodes placed near the exit with a length of L ($0 \leq L \leq 10$ mm). In simulation, the computational region is partitioned with square cells (z_i, r_j) of the size $\Delta z = \Delta r = 0.5$ mm.

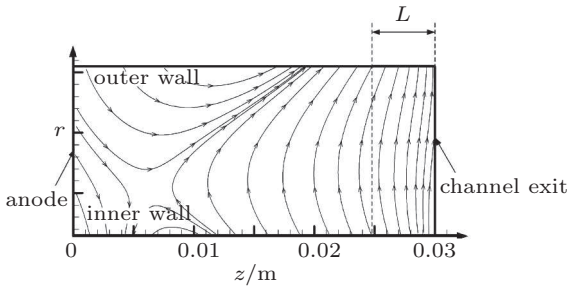


Fig. 1. Computational region, segmented length L, and magnetic field lines used in the model.

To obtain the plasma dynamics, the leapfrog method of Boris version is used.[21] The time step is selected to satisfy $\omega_{pe}\Delta t < 0.3$ and $\omega_{ce}\Delta t < 0.2$, where ω_{pe} and ω_{ce} are the plasma frequency and electron gyro-frequency, respectively. Particle colliding with boundary and with each other are considered in this model.[22] The effective electron collision frequency related to the anomalous transport (Bohm diffusion) $\nu_B = \alpha\omega_{ce}$ is also considered in the model, where $\alpha = 1/64$ is the empirical parameter in Hall thrusters which has been validated by many fluid and hybrid results as shown in Refs. [23] and [24]. Furthermore, the SEE caused by electron–wall collision is considered on both the dielectric (BN) wall surface and the low-emissive electrode (graphite) wall surface. For this purpose, an improved SEE model[25] based on the SEE model given by Morozov is applied. As shown in Fig. 2, $\sigma(\varepsilon_p)$ is the SEE yield caused by single incident electron with energy ε_p. The chosen parameters make the SEE model accord well with the experimental results. In addition, the secondary electrons are emitted, obeying a half Maxwellian distribution.

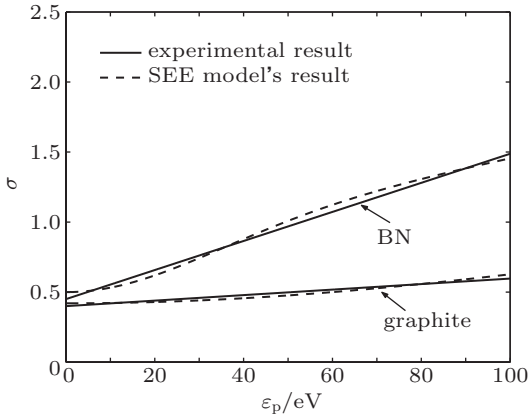


Fig. 2. Comparison of SEE yield between SEE yield model and experimental data.

To solve the electric potential distribution, the dynamic alternating direction implicit (DADI) method is used to solve Poisson equation.[26] The electric potentials at the anode and the exit are set to be U_d and zero, respectively. The corresponding boundary conditions for electric potential ϕ at inner and outer dielectric walls are[27]

inner dielectric wall:

$$\frac{\phi_{i-1,j}-2\phi_{i,j}+\phi_{i+1,j}}{\Delta z^2}+\frac{2\phi_{i,j+1}-2\phi_{i,j}}{\Delta r^2} = -\frac{1}{\varepsilon_0}\left(\rho_{i,j}+\sigma_{i,j}/\Delta r\right), \tag{1a}$$

outer dielectric wall:

$$\frac{\phi_{i-1,j}-2\phi_{i,j}+\phi_{i+1,j}}{\Delta z^2}+\frac{2\phi_{i,j-1}-2\phi_{i,j}}{\Delta r^2} = -\frac{1}{\varepsilon_0}\left(\rho_{i,j}+\sigma_{i,j}/\Delta r\right), \tag{1b}$$

where $\rho_{i,j}$ is the space charge density, $\sigma_{i,j}$ the surface charge density, and ε_0 the vacuum permittivity. As to the potential on the floating conductive wall surface, Szabo[20] presented a simple model

$$\Phi_{\rm s}=\frac{Q_{\rm s}}{C}, \tag{2}$$

where $Q_{\rm s}$ is the net charge deposited on the wall, and the capacitance $C=10^{-10}$ F.

The magnetic field used in the simulation is obtained with the Finite Elements Method Magnetics (FEMM),[28] which is a user-friendly magnetic field solver available on the internet. The typical magnetic field topology is shown in Fig. 1.

In order to accelerate the simulation, a one-dimensional fluid equation is used to calculate the distribution of neutral density $n_{\rm a}$ along the channel axis[29]

$$v_{\rm az}\frac{\partial n_{\rm a}}{\partial z}=-\nu_{\rm ionize}n_{\rm a}+\nu_{\rm recom}, \tag{3}$$

where the axial neutral velocity $v_{\rm az}$ is fixed at 105 m/s based on experimental measurement,[9,30] $\nu_{\rm ionize}$ is the ionization frequency and $\nu_{\rm recom}$ the ion volume-recombination frequency on the two lateral walls within unit axial channel volume. Since we only care about the steady-state, the time term partial derivative is ignored. The geometrical scaling method[30] is also adopted here with a geometrical scaling factor 0.02.

Some parameters used in simulation are set as follows. The anode potential $U_{\rm d}$ is 350 V, the temperature of the introduced electrons on the right boundary is 5 eV; the emission temperature of secondary electrons is 1 eV. The Xenon mass flow rate is 2 mg/s.

3. Results and analysis

By implementing the numerical model described in Section 2 for the cases of segmented electrode length $L=0$, 3, 5, 8 mm, we obtain the main physical parameters to reflect the electron–wall interaction in Hall thruster. Different from the theoretical predictions of formal theoretical model in Ref. [8], in which a small total SEE yield is used and the electron–wall interaction should be weakened, our numerical results show that the low-emissive electrode actually enhances electron–wall interaction. As shown in Fig. 3, although the emitted electron flux $S_{\rm w2}$ of wall in the region of electrode is smaller than in the non-segmented electrode case, in the remaining region $S_{\rm w2}$ is obviously larger than that in the non-segmented electrode case. In the whole discharge channel, the maximal value of $S_{\rm w2}$ for the segmented electrode case is 1.1% to 53% times larger than for the non-segmented electrode case.

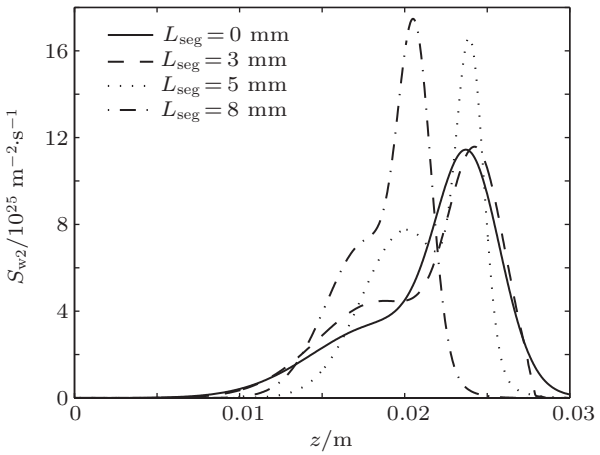


Fig. 3. Axial distributions of emitted electron flux $S_{\rm w2}$ along the inner wall for the cases of segmented electrode length $L=0$, 3, 5, 8 mm.

It is interesting to find the reason for the electron–wall interaction enhancement in the segmented electrode case. Based on formal theories, the electron–wall interaction is to a great extent determined by the total SEE yield δ,[8] which is expressed as

$$\delta=\frac{\Gamma_{\rm se}}{\Gamma_{\rm e}}=\frac{\int_0^\infty\sigma(\varepsilon_{\rm p})vf(v)\,{\rm d}v}{\int_0^\infty vf(v)\,{\rm d}v},$$

where $f(v)$, $v>0$ is the velocity distribution function of incident electron at wall, $\sigma(\varepsilon_{\rm p})$ the SEE yield caused by single electron with energy $\varepsilon_{\rm p}=m_{\rm e}v^2/2$ (see Fig. 2), and $m_{\rm e}$ the mass of electron. It is not difficult to find out that δ is approximately determined by plasma electron temperature $T_{\rm e}$ and wall SEE characteristic, since $\sigma(\varepsilon_{\rm p})$ is approximately proportional to $\varepsilon_{\rm p}$ (see Fig. 2) and $T_{\rm e}$ is significantly correlated with $f(v)$. Furthermore, due to the fact that the enhanced electron–wall interaction for the segmented electrode case appears in the dielectric region (namely $0<z<30-L$), we then conjecture that the increase of electron temperature should be the reason for electron–wall interaction enhancement. From the electron temperature distribution in Fig. 4, we can see that the maximal electron temperature for the segmented electrode case is indeed 0.05 eV–4 eV larger than that for the non-segmented electrode case. In general, the increased electron temperature is attributed to the weakened electron–wall interaction in the region of electrode (as shown in Fig. 3).

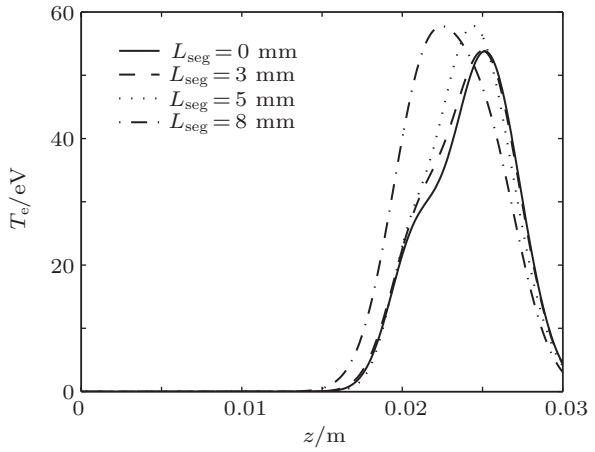


Fig. 4. Axial distributions of electron temperature T_e along the channel central line for the cases of segmented electrode length $L = 0$, 3, 5, 8 mm.

As for the weakening of electron–wall interaction in electrode region (see Fig. 3), one may first attribute it to the low-emissive characteristic of electrode since the low SEE characteristic can increase the sheath potential drop.[8] Besides the low-emissive characteristic, our study shows that the conductivity property of electrode is also a significant factor influencing electron–wall interaction because it makes equipotential lines convex toward channel exit and even parallel to wall in near-wall region (see Fig. 5).[19] This equipotential configuration obviously increases the radial potential drop in near-wall region, and thus repels a mass of electrons, thereby causing the electrons to move toward the channel center. Therefore, both the low-emissive characteristic and the conductive property of electrode are the reason for the weakening of electron–wall interaction in electrode region.

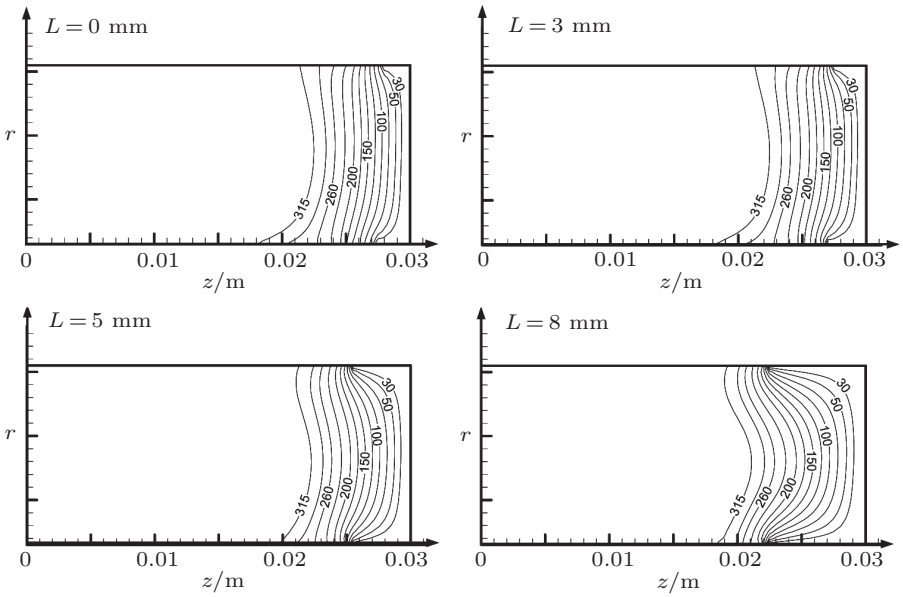


Fig. 5. Spatial distributions of equipotential lines in discharge channel for the cases of segmented electrode length $L = 0$, 3, 5, 8 mm.

Although the segmented electrode weakens the electron–wall interaction in the segmented region, thus enhancing the maximal electron temperature in discharge channel, the propellant ionization rate S_i of the segmented electrode case does not increase for all the segmented electrode cases compared with that of the non-segmented electrode case (shown in Fig. 6). As for the xenon propellant, the axial ionization rate can be expressed as[31]

$$S_i(z) = \begin{cases} 0, & T_e < T^*, \\ n_a(z) n_e(z) \beta_0(z) \left(\dfrac{T_e}{T^*} - 1 \right), & T_e > T^*, \end{cases} \tag{4}$$

where n_e is the electron density, $\beta_0 = 2.2 \times 10^{-14}$ m^3·s^{-1}, and $T^* = 4$ eV. This relation indicates that when the propellant mass flow rate is fixed. which means that n_a is invariable, S_i is approximately determined by the product of n_e and T_e. In fact, only the electron with relative-high energy can induce the ionization of propellant; and the electron emitted from wall is a significant seed electron that induces atom ionization because the emitted secondary electron is accelerated by the strong radial electric field in the discharge channel. Although the segmented electrodes emit much less secondary electrons than the non-segmented electrode (see Fig. 3), the secondary electrons that are emitted from the electrodes will be significantly accelerated by the radial electric field, thus obtaining an energy even more than 100 eV when they reach the channel center (see Fig. 5). Therefore, we can come to a conclusion that the conductivity property of segmented electrodes that make the equipotential lines convex toward channel exit is the reason for ionization rate S_i increasing in the region of segmented elec-

trode. However, in the remaining region, the maximum value of ionization rate S_i changes non-monotonically with the increase of segmented electrode length L. The reason for the non-monotonic variation of S_i in the region of dielectric channel is that, on the one hand, the increased ionization rate S_i in the region of segmented electrode generates a mass of electrons that will be accelerated and enter into the region of dielectric channel, but meanwhile the electron in discharge channel loses much energy in the ionization process of segmented electrode region on the other hand.

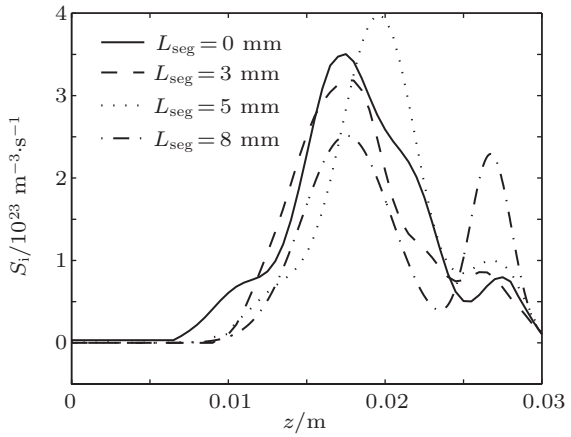


Fig. 6. Axial distributions of propellant ionization rate S_i for the cases of segmented electrode length $L = 0$, 3, 5, 8 mm.

The segmented electrode also has a significant influence on discharge current I_d. As shown in Fig. 7, discharge current I_d is obviously enhanced for the segmented electrode case, which is qualitatively in accordance with the results of formal experiments in Ref. [16]. With the increase of segmented electrode length L, I_d increases monotonically. In general, there are two reasons for the increase of discharge current: the first one is the enhanced electron–wall interaction (shown in Fig. 3) which causes a relatively large NWC current, and the second one is the conductivity current in the surfaces of segmented electrodes. Based on Ref. [10], the short-circuit current through the conductive walls is neutralized by the ions collected all over the surfaces of the electrodes, and this short-circuit current can be expressed as

$$I_{sc} = e \int_S I_{wi} \, dS, \tag{5}$$

where S is the electrode area of plasma-facing surface, I_{wi} the density of ion current collected from the wall. Because the convex equipotential configuration results in ion beam defocusing,[19] both the ion current density I_{wi} and the short-circuit current I_{sc} should increase. As shown in Fig. 7, I_{sc} increases monotonically with the increase of L.

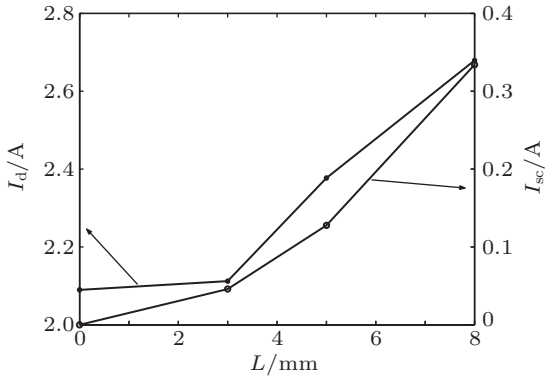


Fig. 7. Discharge current I_d and short-circuit current I_{sc} versus segmented electrode length L.

4. Conclusions

Making use of a fully kinetic PIC method to simulate the two-dimensional plasma flow, we investigate the electron–wall interaction in an Aton-type Hall thruster with segmented electrodes placed near the exit of discharge channel. The results show that the low-emissive characteristic weakens the electron–wall interaction in the region of segmented electrode; the conductive property of segmented electrode tends to make equipotential lines convex toward channel exit and even parallel to wall in near-wall region, which further weakens the electron–wall interaction in the region of segmented electrode by repelling a mass of electrons, thus causing the electrons to move toward the channel center. The convex equipotential configuration also causes the propellant ionization rate to increase in the region of segmented electrode by significantly accelerating the secondary electrons. Because the electron–wall interaction is seriously weakened and the ionization rate is increased in the region of segmented electrode, both electron temperature and the number of electrons with relatively high energy are increased in discharge channel, which makes the electron–wall interaction in the remaining region of discharge channel enhanced remarkably. We also find that the discharge current for the segmented electrode case is obviously larger than that for the non-segmented electrode case, which is attributed to the short-circuit current in electrodes and the enhanced electron–wall interaction in the remaining dielectric region.

References

[1] Kim V 1998 *J. Propul. Power* **14** 736
[2] Zhurin V V, Kaufman H R and Robinson R S 1999 *Plasma Sources Sci. Technol.* **8** 1
[3] Morozov A I 1968 *Prikl. Mekh. Tekh. Fiz.* **3** 19
[4] Morozov A I and Savelév V V 2001 *Plasma Phys. Rep.* **27** 570
[5] Zhang F K, Ding Y J, Qing S W and Wu X D 2011 *Chin. Phys. B* **20** 125201
[6] Raitses Y, Staack D, Keidar M and Fisch N J 2005 *Phys. Plasmas* **12** 057104
[7] Mazouffre S, Echegut P and Dudeck M 2007 *Plasma Sources Sci. Technol.* **16** 13
[8] Hobbs G D and Wesson J A 1967 *Plasma Phys.* **9** 85

[9] Keidar M, Boyd I D and Beilis I I 2001 *Phys. Plasmas* **8** 5315

[10] Gascon N, Dudeck M and Barral S 2003 *Phys. Plasmas* **10** 4123

[11] Meezan N B, Gascon N and Cappelli M A 2001 27*th International Electric Propulsion Conference* (Worthington: Electric Rocket Propulsion Society) IEPC-01-039

[12] Raitses Y, Dorf L A, Litvak A A and Fisch N J 2000 *J. Appl. Phys.* **88** 1263

[13] Morozov A I and Savel'ev V V 2000 in *Reviews of Plasma Physics*, ed. Kadomtsev B B and Shafranov V D (New York: Consultants Bureau) Vol. 21

[14] Fisch N J, Raitses Y, Dorf L A and Litvak A A 1999 *AIAA Paper* AIAA-2572

[15] Fruchtman A, Fisch N J and Raitses Y 2001 *Phys. Plasmas* **8** 1048

[16] Staack D, Raitses Y and Fisch N J 2003 *Proceedings of the* 28*th International Electric Propulsion Conference* (Cleveland, OH: Electric Rocket Propulsion Society) IEPC–157

[17] Yu D R, Li J, Liu H, Ning Z X and Li Y 2009 *Contrib. Plasma Phys.* **49** 413

[18] Yu D R, Wei L Q, Li H, Li Y and Jiang B H 2009 *Plasma Sci. Technol.* **11** 714

[19] Yu D R, Qing S W, Liu H and Li H 2011 *Contrib. Plasma Phys.* **51** 955

[20] Szabo J J 2001 Ph. D. thesis, Massachusetts Institute of Technology, USA

[21] Birdsall C K and Langdon A B 1991 *Institute of Physics Publishing* (Bristol and Philadelphia)

[22] Liu H, Yu D R, Yan G J and Liu J Y 2008 *Contrib. Plasma Phys.* **48** 603

[23] Fife J M 1998 Ph. D. thesis Massachusetts Institute of Technology, USA

[24] Koo J W and Boyd I D 2004 *Comput. Phys. Commun.* **164** 442

[25] Yu D R, Zhang F K, Liu H, Li H, Yan G J and Liu J Y 2008 *Phys. Plasmas* **15** 104501

[26] Doss S and Miller K 1979 *Siami. Numer. Anal.* **16** 837

[27] Matyash K, Schneider R, Mutzke A, Kalentev O, Taccogna F, Koch N and Schirra M 2010 *IEEE Trans. Plasma Sci.* **38** 2274

[28] FEMM 2004 *Finite Element Method Magnetics* (Software Package, Ver.4.0, Foster-Miller, Inc, Boston, MA)

[29] Liu H, Wu B Y, Yu D R, Cao Y and Duan P 2010 *J. Phys. D: Appl. Phys.* **43** 165202

[30] Taccogna F, Longo S, Capitelli M and Schneider R 2005 *Phys. Plasmas* **12** 053502

[31] Morozov A I and Savelév V V 2000 *Plasma Phys. Rep.* **26** 875